Supporting Information

Calcium Chloride as an Ionic Response Modulator in Metal Organic Framework-filled Nanopores (MOF@SSNs): Enhancing Ionic Current Saturation and Selectivity

Angel L. Huamani,[a,b] Gregorio Laucirica,[a,c] Juan A. Allegretto,[d] Maria Eugenia Toimil- Molares,[e] Agustin Picco,[a] Marcelo R. Ceolín,[a] Aline R. Passos,[f] Omar Azzaroni,[a] Waldemar A. Mamisolle,[a,*] and Matias Rafti.[a,*]

[a] *Instituto de Investigaciones Fisicoquímicas Teóricas y Aplicadas (INIFTA), Dpto. de Química, Fac. Cs. Exactas, UNLP, CONICET – CC 16 Suc. 4, 1900 La Plata, Argentina.*

(co-corresponding authors mrafti@quimica.unlp.edu.ar and wmarmi@inifta.unlp.edu.ar)

[b] *3IA-UNSAM-CONICET, Instituto de Investigación e Ingeniería Ambiental, Escuela de Hábitat y Sostenibilidad, San Martín, Argentina.*

[c] *UCAM-SENS, Universidad Católica San Antonio de Murcia, UCAM HiTech, 30107 Murcia, Spain.*

[d] *Laboratory for Life Sciences and Technology (LiST), Department of Medicine, Faculty of Medicine and Dentistry, Danube Private University, 3500 Krems, Austria.*

[e] *GSI Helmholtzzentrum für Schwerionenforschung, 64291 Darmstadt, Germany.*

[f] *Brazilian Synchrotron Light Laboratory (LNLS), Brazilian Center for Research in Energy and Materials (CNPEM), Campinas, SP, Brazil.*

-OP-synthesis for UiO-66-modified membranes

The One-Pot synthesis for UiO-66 in nanochannels employed the same physical setup as CD. The specific process of filling the Teflon cells is illustrated in **Figure 2(a)**. Two separate solutions were initially prepared: 0.1540 g of ZrCl$_4$ in 8.7 mL of DMF and 1.3 mL of HCl, and 0.1560 g of BDC in 10.0 mL of DMF. Post-sonication for two minutes each, these solutions were combined in equal volumes. This unified mixture was then introduced into both Teflon cell reservoirs. The OP process also entailed an overnight incubation at 80°C. Following this, the membrane cleaning protocol was identical to that of the CD method, involving sequential washes with fresh DMF and EtOH, and a concluding two-hour immersion in Milli-Q water.

-Top-Views SEM images
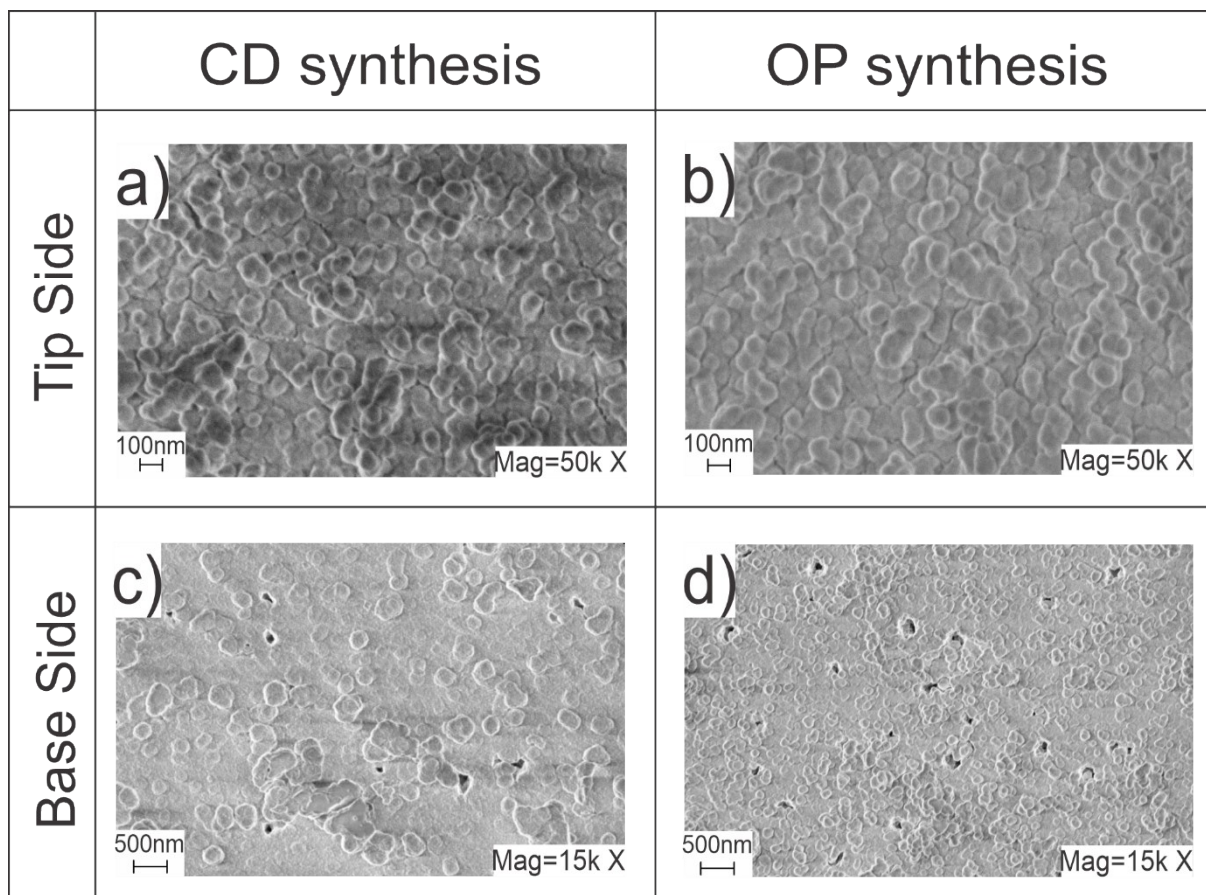
Figure S1. Top-view SEM images of both sides of UiO-66@PET membranes for both CD synthesis and OP synthesis

-Preliminary Ptychographic X-ray computed tomograph

Preliminary ptychography experiments were performed at the Brazilian Synchrotron Light Laboratory (LNLS-Sirius, Campinas-SP, Brazil. Proposal ID: 20222053).[1,2] The measurements were conducted using a 6 keV X-ray beam. To obtain an isolated specimen for ptychography measurements, the samples were cut using a laser microdissection microscope (Leica LMD7) achieving specimens of approximately 30 μm in height. The samples were transferred to silicon nitride membranes with thickness of 100 nm. These membranes were placed in the experimental hutch of the Cateretê beamline and aligned with the help of an optical microscope. Diffraction patterns were collected using a PiMega540D detector at a sample-detector distance of 15 m. The illumination on the sample was defined by a 10 μm diameter pinhole. The position trajectories for each 2D scan were defined using a grid with an average

step size of 2 μm, covering a field of view of 44x 44 μm^2. For tomography, the field of view covered for each projection was 44 x 30 μm^2, 920 projections were collected with a total angular of 154°. 2D and 3D ptychographic reconstructions were performed with the code developed by the Scientific Computing Group (GCC) of Sirius. Segmentation to separate the polymeric matrix from the porous structure was performed using Avizo software (Thermo Scientific™). The images were segmented using a threshold based on gray level values.

Figure S2 presents 2D/3D X-Ray ptychography results from the bare PET membrane (10^6 pores/cm^2) under study. **Figure S2(a)** shows the 2D electron density projections reconstructed with 19.4 nm pixel size. The ptychographic X-ray computed tomography was performed to quantify the pore structure in a selected region of interest. The 3D volume rendering from the front view and the bottom view are presented in the **Figure S2(b) and (c)**, respectively. The irregular shape of pores in the membrane surface may be related to the damage caused by the laser microdissection used in the sample preparation. This effect is more pronounced near the edges of the membrane. **Figure S2(d)** shows the selected slice of the 3D volume, the segmented pore diameter was ca. 370 nm in the inner part of the pore. The total thickness was ca. 12 μm. Quantitative label analysis also allowed to determine the pore volume of 6.08 μm^3. As observed, the overall shape of the pore deviates from the bullet shape observed by SEM. Again, we speculate that this may be a consequence of the damage caused by the microdissection.
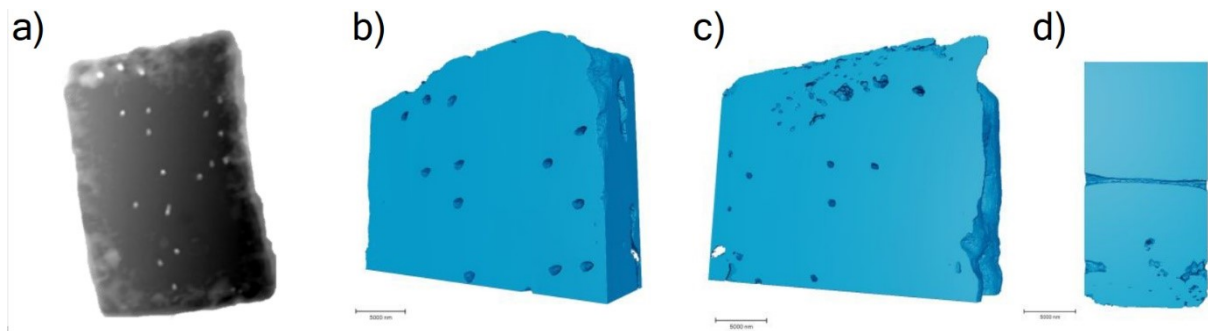

Figure S2. Ptychographic X-ray computed tomography results: a) 2D electron density of a single projection. b) 3D volume rendering showing the slightly tilted front view (base side) and c) the bottom view (tip side). d) selected slices of the 3D volume rendering showing a pore across the membrane. Scale bars refers to 5000 nm.

-Electrochemical setup
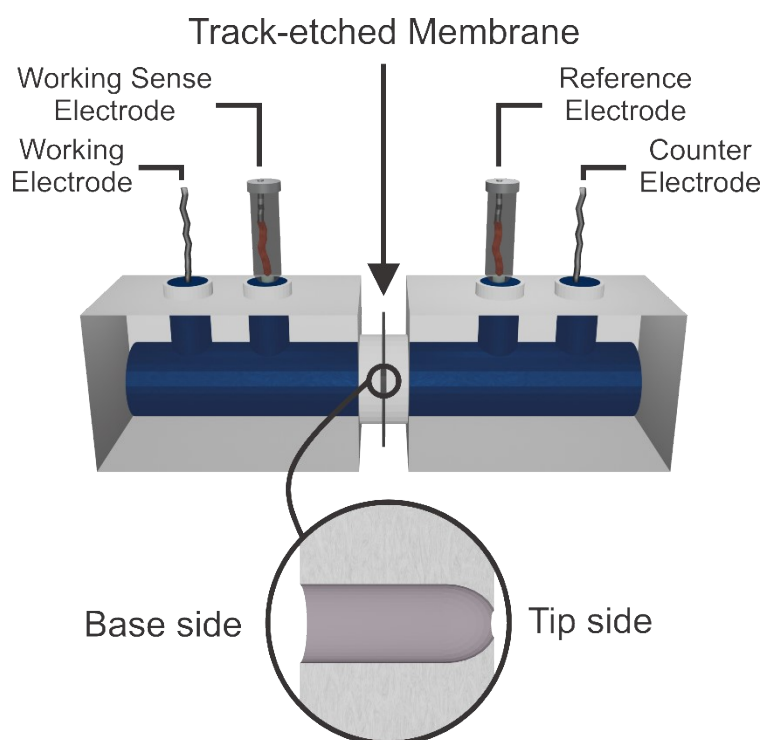
Figure S3. Scheme of the experimental setup for performing electrochemical measurements with the membranes. Inset: Membrane position in all measurements.

Iontronic Response of bare bullet-shaped nanochannels
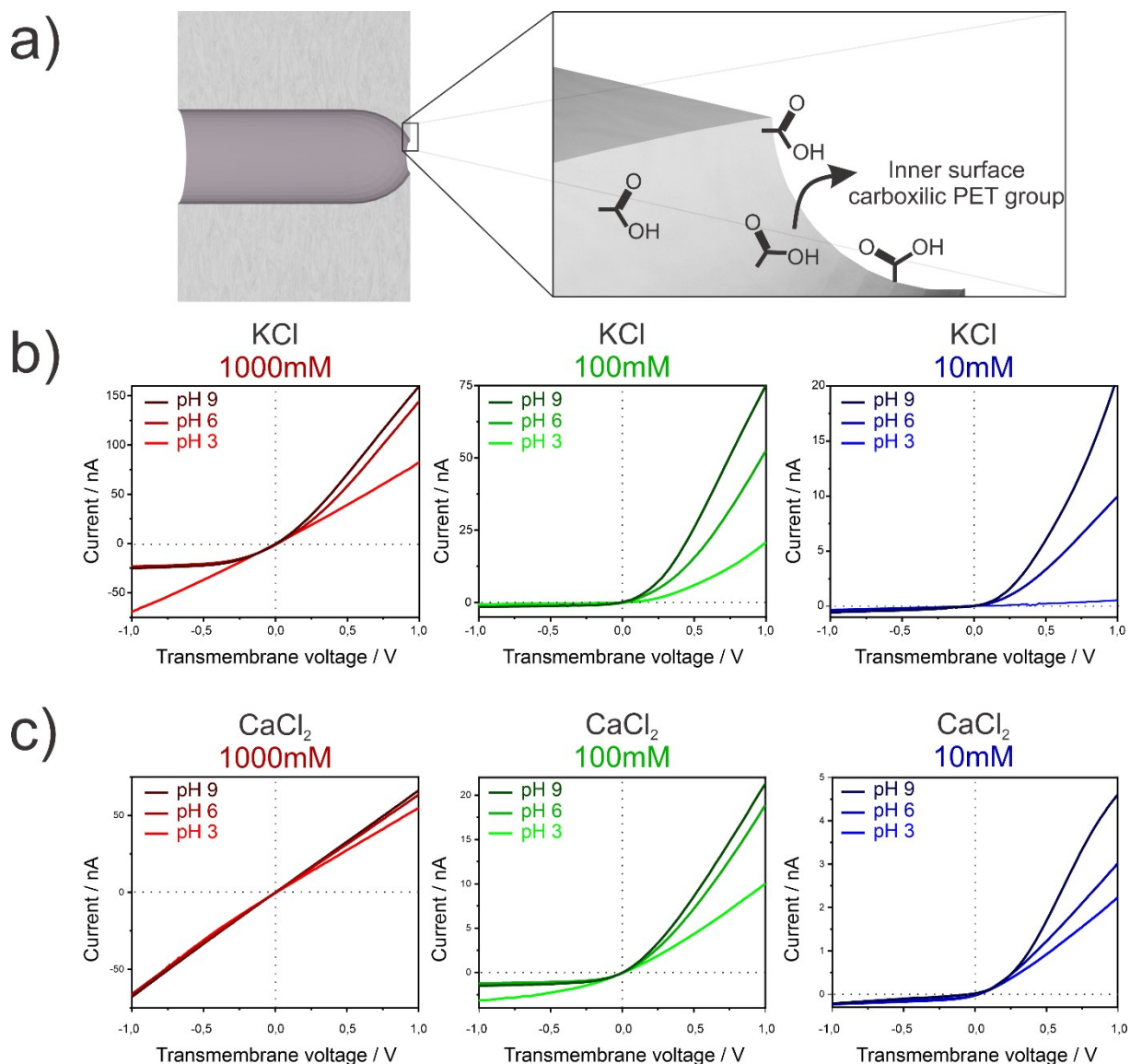
Figure S4. a) Bare bullet-shaped nanochannel after the etching process. Inset: Carboxylic groups responsible for the negative charge within the nanochannel. b) KCl response at various concentrations and pH levels. c) CaCl₂ response at different concentrations and pH values.

Iontronic Response of OP-Synthesized Membranes

As previously discussed, the membranes modified by OP synthesis exhibit typical pH-dependent rectification behavior, as shown in **Figure S5**. These membranes show a charge inversion when KCl is used, but do not exhibit charge inversion with CaCl$_2$, indicating a positive surface charge of the channel even at basic pH levels.
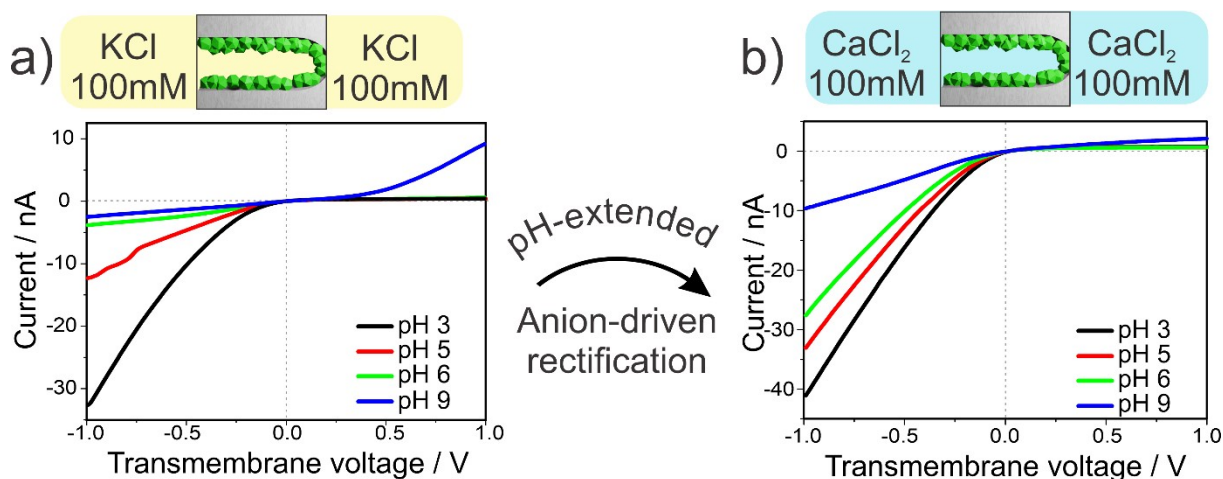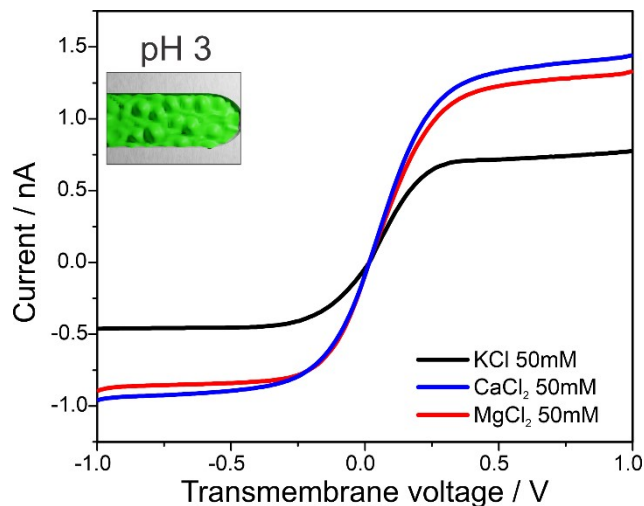
Figure S5. I-V curves for OP-synthesized UiO-66-modified membrane in a) 100 mM KCl solution and b) 100 mM CaCl$_2$ solution at different pH values.

The lack of current saturation in the presence of CaCl$_2$ for OP synthesis can be rationalized by taking into account the presence of large lumens in the nanochannels, different from the CD close packing featuring constructional porosity. Summarizing, loosely packed OP-synthesized membranes exhibit, upon functionalization with Ca^{2+}, a surface charge increases which is not enough to provoke diffusion-limited ionic transport needed for the ICS regime stablished in CD-synthesized membranes.

Magnesium effect on the ionic transport

Having demonstrated the influence of calcium ions on the ionic transport in MOF-decorated SSNs, and the affinity of calcium ions (ex-situ) for the MOF material, we studied the effect of another divalent cation: Magnesium (Mg^{2+}). The study of the effect of CaCl$_2$ electrolyte on the iontronic response of UiO-66- filled SSNs revealed that the ionic current for Ca^{2+} significantly surpassed that of K$^+$, a rarity in such contexts.[3,4]

Further experiments using MgCl$_2$ as an electrolyte (**Figure S6**) showed an iontronic behavior similar to that observed with CaCl$_2$. The consistent ionic currents generated by both MgCl$_2$ and CaCl$_2$, exceeding those of KCl at the same concentration, align with their bulk mobility values (5.97 and 6.17 x 10^{-8} m^2 V^{-1}s^{-1} for Mg^{2+} and Ca^{2+}, respectively). Despite the highly negative hydration energies of Mg^{2+} and Ca^{2+}(-1929 and -1579 kJ/mol, respectively)[5] and their large hydration diameters (0.824 nm and 0.856 nm, respectively)[6] compared to the window size connecting the pores of UiO-66 (0.6 nm), the lack of significant difference in their behavior within the nanochannels, added to the previously exposed results in **Figures 4-6**, confirms that the primary transport mechanism involves the constructional porosity and not the microporosity of the MOF. Instead, the comparable behavior indicates that both ions traverse the constructional porosity within the channels, where they interact with the positively charged environment created by their own binding to the free-carboxylate groups in the MOF structure without losing their hydration sphere and compromising the microporosity of the MOF

Figure S6. I-V curves CD-synthesized UiO-66-modified membrane in the presence of different electrolytes at pH=3

-XRD measures

The obtained diffraction patterns (**Figure S7**) showcase the expected peaks for UiO-66 MOF with a fcu topology (2θ = 7.5°, 8.5°, and 25.8°), with no changes upon exposure to the different media.[7] This correspondence indicates that the crystalline structure of the UiO-66 MOF is adequately preserved after the treatments with different salts, with no evidence of alteration in the material's structural integrity.
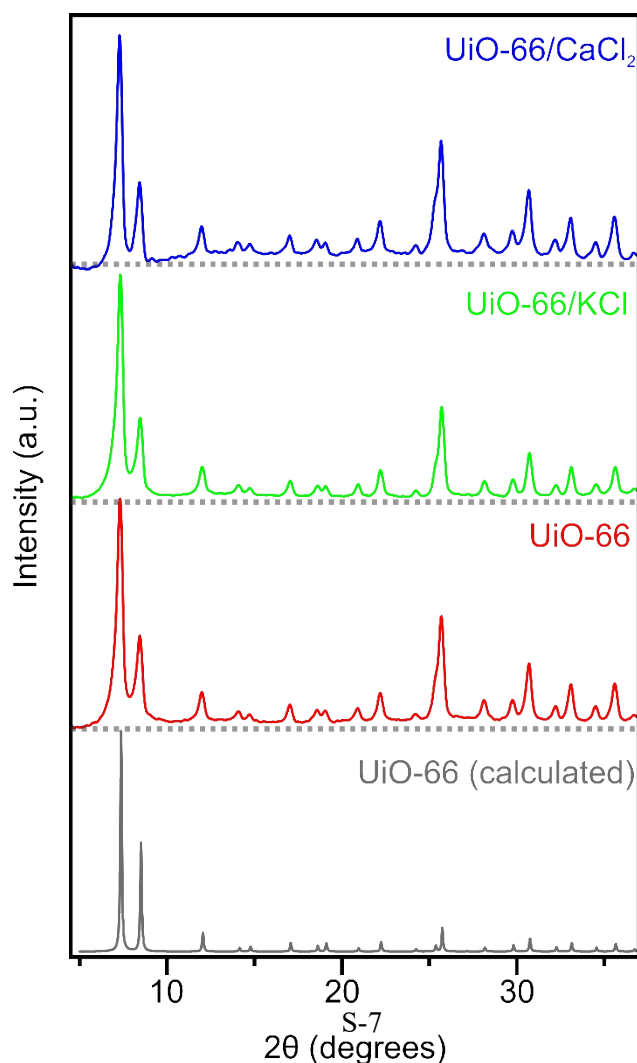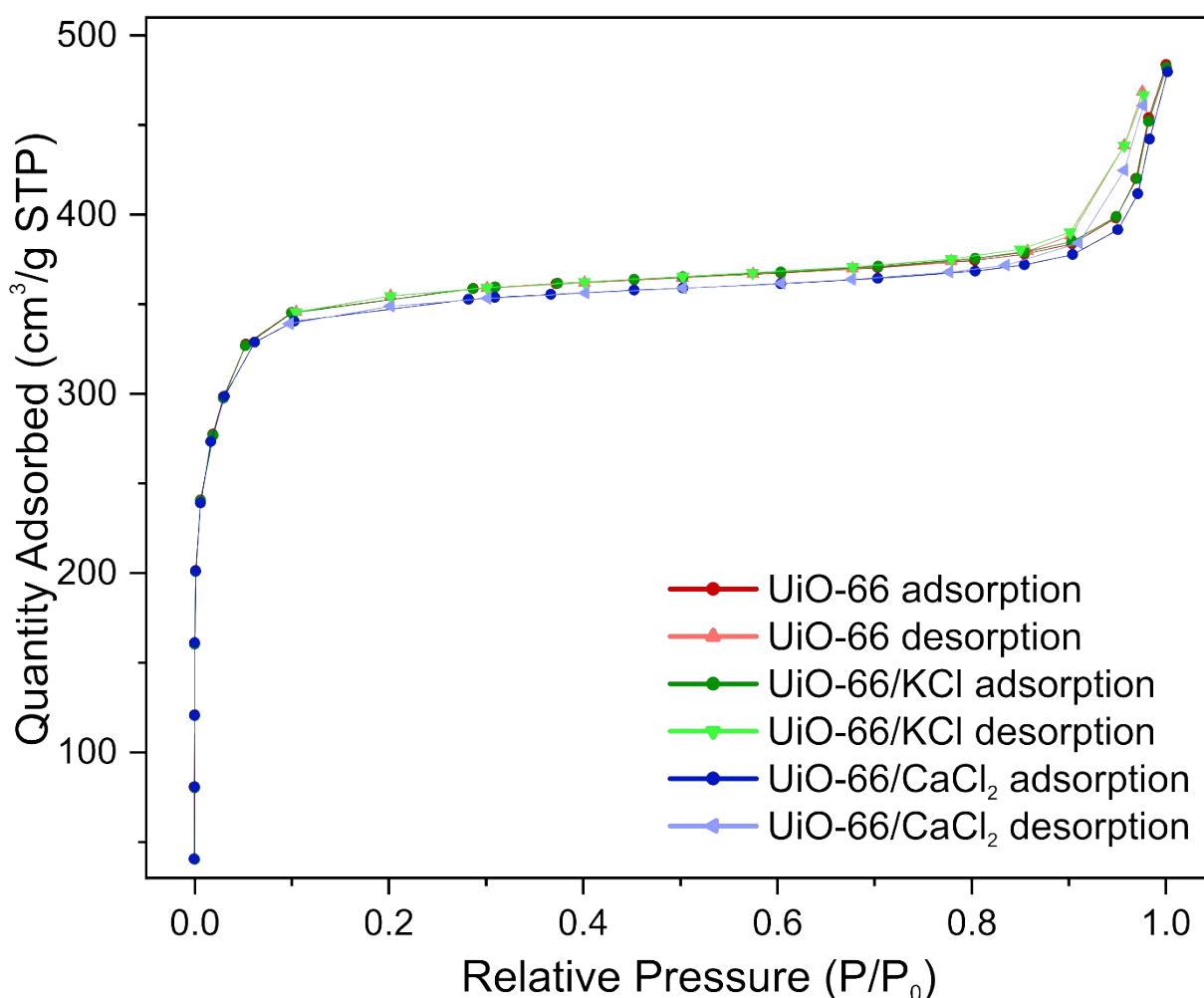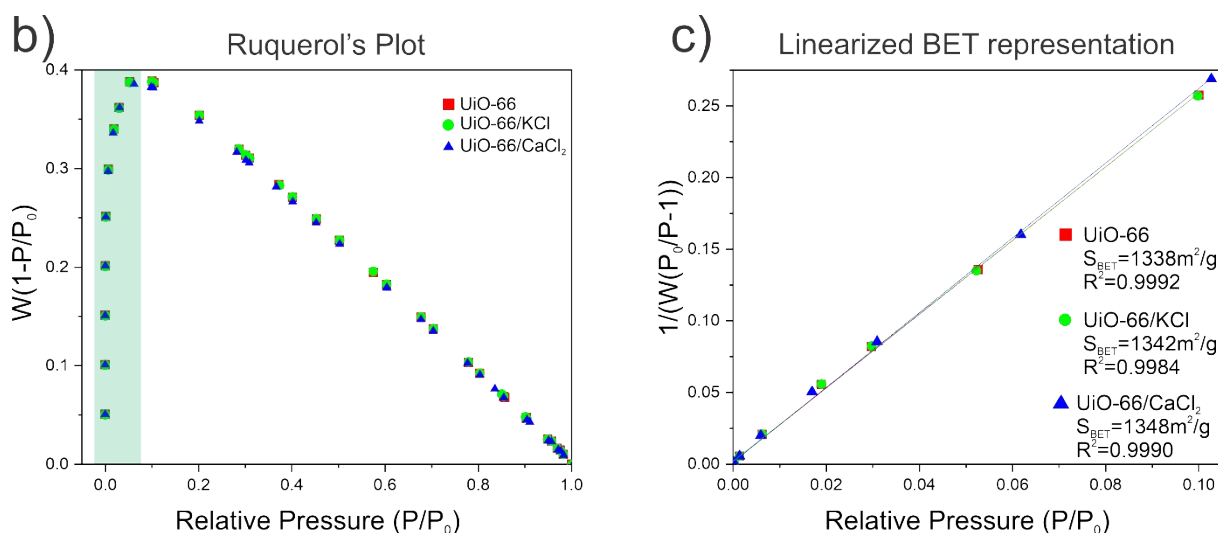
Nitrogen adsorption isotherms

N_2 adsorption-desorption isotherms at 77 K were conducted to explore the porosity of the UiO-66 sample and its variants exposed to KCl and $CaCl_2$ (**Figure S8(a)**). The Rouquerol analysis (**Figure S8(b)**) was employed to select the optimal range of relative pressure, as indicated in the green-shaded region. The linearized BET technique (**Figure S8(c)**) revealed that the specific surface areas of the modified materials remain constant within the error margin of the method, suggesting that the modification does not alter the essential microporosity of UiO-66. The BET constant (C), obtained from the slope of the linearized graph, along with the BET equation and N_2 molecular parameters, allowed for the calculation of specific surface area, confirming the post-modification structural consistency.

a) **N$_2$ adsorption-desorption isotherm at 77 K for UiO-66 powder**

Figure S8. a) N_2 adsorption isotherms at 77K. b) Rouquerol's plot employed for BET analysis pressure range determination. c) Linearized BET representation and surface areas obtained.

-Thermogravimetric analysis

Subsequent analysis uncovered disparities among the samples, indicating selective ionic adsorption within the UiO-66 framework after exposure to saline solutions, as illustrated in **Figure S9**. Notably, the final residue differences showed deviations of up to 5% compared to the untreated MOF, suggesting the incorporation of K^+ or Ca^{2+} ions, as described in MOFs under analogous conditions.[8] However, the technique's error margin does not allow differentiation between both modified samples.
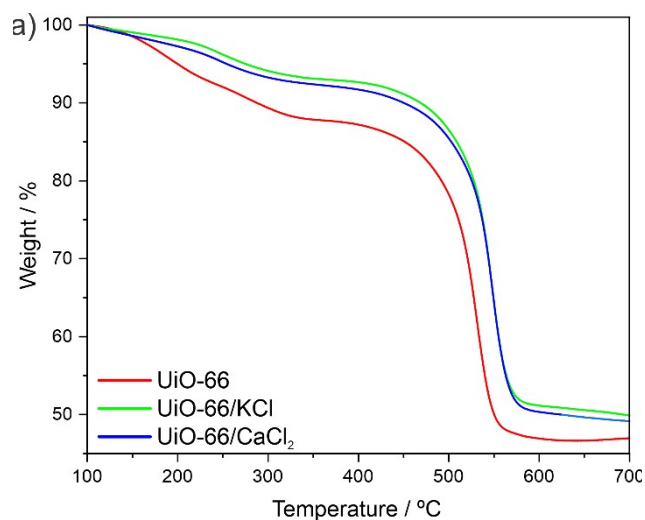

Figure S9. TGA curves for UiO-66 powder samples.

-FTIR

Spectral bands that remained unchanged across all samples were identified, attributed to the carbon skeleton vibrations of the ligand, exemplified by the band at 1507 cm^{-1} associated with aromatic C-C stretching.[9,10]

As discussed in the main manuscript, and illustrated in **Figure S10**, there are not changes in the bands associated with the ZrO cluster, such as the one appearing at 554 cm^{-1} for the samples containing the MOF. This band is associated with Zr-(OC) asymmetric stretching.[11] These findings collectively suggest that the modification with CaCl$_2$ primarily involves the incorporation of Ca^{2+} ions into the MOF through complexation with the MOF free carboxylic groups, identified as the most probable site due to the detected spectral differences. Additionally, it is concluded that the interaction of Ca^{2+} ions with the ZrO cluster does not occur.
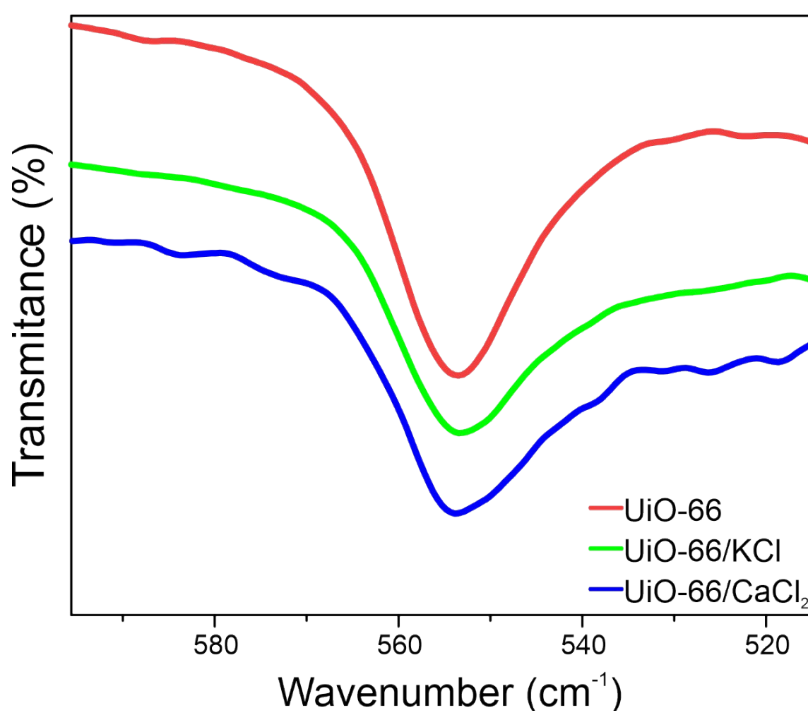
Figure S10. FTIR Spectra Focused on the Asymmetric Stretching Zone of Zr-(OC) asymmetric stretching.

References

1. *Acta Crystallographica Sect. A Found. Adv.*, 2021, **77**, C283.
2. R. Górecki, C. C. Polo, T. A. Kalile, E. X. S. Miqueles, Y. R. Tonin, L. Upadhyaya, F. Meneau, S. P. Nunes, Ptychographic X-ray computed tomography of porous membranes with nanoscale resolution, *Commun. Mater.*, 2023, **4**, 68.
3. J. Lu, H. Zhang, J. Hou, X. Li, X. Hu, Y. Hu, C. D. Easton, Q. Li, C. Sun, A. W. Thornton, M. R. Hill, X. Zhang, G. Jiang, J. Z. Liu, A. J. Hill, B. D. Freeman, L. Jiang, H. Wang, Efficient metal ion sieving in rectifying subnanochannels enabled by metal–organic frameworks, *Nat. Mater.*, 2020, **19**, 767–774.
4. J. Hou, H. Zhang, J. Lu, X. Li, C. Zhao, H. Wang, A. W. Thornton, K. Konstas, Influence of surface chemistry and channel shapes on the lithium-ion separation in metal-organic-framework-nanochannel membranes, *J. Memb. Sci.*, 2023, **674**, 121511.
5. D. W. Smith, Ionic hydration enthalpies, *J. Chem. Educ.*, 1977, **54**, 540.
6. D. Jiao, C. King, A. Grossfield, T. A. Darden, P. Ren, Simulation of Ca2+ and Mg2+ Solvation Using Polarizable Atomic Multipole Potential, *J. Phys. Chem. B*, 2006, **110**, 18553–18559.
7. L. Valenzano, B. Civalleri, S. Chavan, S. Bordiga, M. H. Nilsen, S. Jakobsen, K. P. Lillerud, C. Lamberti, Disclosing the Complex Structure of UiO-66 Metal Organic Framework: A Synergic Combination of Experiment and Theory, *Chem. Mater.*, 2011, **23**, 1700–1718.

8. G. Zhang, F. Xie, T. M. Osborn Popp, A. Patel, E. M. Cedeño Morales, K. Tan, R. Crichton, G. Hall, J. Zhang, A. J. Nieuwkoop, J. Li, A series of cation-modified robust zirconium-based metal–organic frameworks for carbon dioxide capture, *CrystEngComm*, 2023, **25**, 1067–1075.
9. S. Agatonovic-Kustrin, K. S. Balyklova, V. Gegechkori, D. W. Morton, HPTLC and ATR/FTIR Characterization of Antioxidants in Different Rosemary Extracts, *Molecules*, 2021, **26**, 6064.
10. J. Zhuang, M. Li, Y. Pu, A. Ragauskas, C. Yoo, Observation of Potential Contaminants in Processed Biomass Using Fourier Transform Infrared Spectroscopy, *Appl. Sci.*, 2020, **10**, 4345.
11. L. Valenzano, B. Civalleri, S. Chavan, S. Bordiga, M. H. Nilsen, S. Jakobsen, K. P. Lillerud, C. Lamberti, Disclosing the Complex Structure of UiO-66 Metal Organic Framework: A Synergic Combination of Experiment and Theory, *Chem. Mater.*, 2011, **23**, 1700–1718.